


Cite this: *Chem. Sci.*, 2023, 14, 1590

All publication charges for this article have been paid for by the Royal Society of Chemistry

## Understanding the role of ring strain in $\beta$ -alkyl migration at Mg and Zn centres†

Joseph M. Parr, Andreas Phanopoulos, Aaranjah Vickneswaran and Mark R. Crimmin \*

The activation of C–C  $\sigma$ -bonds within strained three- and four-membered hydrocarbons at electrophilic Mg and Zn centres is reported. This was achieved in a two-step process involving (i) hydrometallation of a methyldene cycloalkane followed by (ii) intramolecular C–C bond activation. While hydrometallation of methyldene cyclopropane, cyclobutane, cyclopentane and cyclohexane occurs for both Mg and Zn reagents, the C–C bond activation step is sensitive to ring size. For Mg, both cyclopropane and cyclobutane rings participate in C–C bond activation. For Zn, only the smallest cyclopropane ring reacts. These findings were used to expand the scope of catalytic hydrosilylation of C–C  $\sigma$ -bonds to include cyclobutane rings. The mechanism of C–C  $\sigma$ -bond activation was investigated through kinetic analysis (Eyring), spectroscopic observation of intermediates, and a comprehensive series of DFT calculations, including activation strain analysis. Based on our current understanding, C–C bond activation is proposed to occur by a  $\beta$ -alkyl migration step.  $\beta$ -Alkyl migration is more facile for more strained rings and occurs with lower barriers for Mg compared to Zn. Relief of ring strain is a key factor in determining the thermodynamics of C–C bond activation, but not in stabilising the transition state for  $\beta$ -alkyl migration. Rather, we ascribe the differences in reactivity to the stabilising interaction between the metal centre and the hydrocarbon ring-system, with the smaller rings and more electropositive metal (Mg) leading to a smaller destabilisation interaction energy as the transition state is approached. Our findings represent the first example of C–C bond activation at Zn and provide detailed new insight into the factors at play in  $\beta$ -alkyl migration at main group centres.

Received 15th November 2022

Accepted 7th January 2023

DOI: 10.1039/d2sc06288g

rsc.li/chemical-science

## Introduction

Reactions that break strong carbon–carbon bonds are of broad importance. For example, C–C bond activation is emerging as a fundamental transformation that can be used to achieve skeletal modification of organic molecules, offering a novel approach for synthetic disconnections.<sup>1,2</sup> Reactions that break C–C bonds also underpin our global energy sector. Catalytic cracking of C–C bonds in hydrocarbon feedstocks, such as crude oil, converts high molecular weight alkanes to more valuable alkenes and medium-length hydrocarbons (*e.g.* C<sub>7</sub> to C<sub>9</sub> alkanes). Breaking C–C bonds is, unsurprisingly, very challenging. C–C bonds are ubiquitous but strong and non-polar. The bonding orbitals associated with C–C bonds are often sterically congested, making them kinetically inaccessible. Take for instance, the bonds found in alkanes: the C–C bond of CH<sub>3</sub>–CH<sub>3</sub> has a homolytic bond dissociation energy of 90.1  $\pm$

0.1 kcal mol<sup>−1</sup>.<sup>3</sup> Chemoselectivity further complicates C–C bond activation, with surrounding C–H bonds often the first sites to react.

C–C bond activation has been achieved on the surface of heterogeneous catalysts,<sup>4</sup> within the active sites of enzymes,<sup>5</sup> and under homogeneous conditions using metal complexes.<sup>6,7</sup> Reported reactivity typically employs a late transition metal (Rh, Ir, Pd, Pt) as part of the active site for C–C activation.<sup>8</sup> Reactivity often follows classical mechanisms, divided into two broad classes: (i) the direct oxidative addition of the transition metal to the C–C bond;<sup>9</sup> (ii)  $\beta$ -alkyl elimination at a metal centre (Fig. 1);<sup>10</sup>  $\beta$ -alkyl migration can be defined as a sub-class of  $\beta$ -alkyl elimination, wherein the substrate remains intact on the transition metal throughout the pathway.

There is an urgent requirement for more sustainable approaches to this fundamental transformation through replacement of the rare and expensive transition metals often used for bond breaking. To that end, main-group metals have been investigated toward C–C activation. Main-group metals are light, non-toxic alternatives that are abundant and readily accessible; common examples include Al, Mg, and Zn. Though limited, some notable contributions toward main-group C–C bond activation have been reported.

Molecular Sciences Research Hub, Department of Chemistry, Imperial College London, 82 Wood Lane, White City, Shepherd's Bush, London, W12 0BZ, UK. E-mail: m.crimmin@imperial.ac.uk

† Electronic supplementary information (ESI) available. CCDC 2211702–2211705. For ESI and crystallographic data in CIF or other electronic format see DOI: <https://doi.org/10.1039/d2sc06288g>



Crystals of **5b** and **5c** suitable for single crystal X-ray diffraction were grown from *n*-pentane solution (Fig. 2). Both structures show the expected three-coordinate geometry at zinc supported by the  $\beta$ -diketiminate ligand and a hydrocarbon fragment that contains the intact carbocycle. The bond lengths to Zn are consistent with related structures and largely unremarkable.<sup>23–27</sup> The sum of the N–Zn–N, N–Zn–C, and C–Zn–N bond angles for both is close to 360° for both **5b** (359.96(12)°) and **5c** (359.99(24)°) suggestive of  $sp^2$  hybridisation and coordinative unsaturation at the metal. The nearest approach of the centroid of the C <sup>$\beta$</sup> –C <sup>$\gamma$</sup>  bond to the metal is beyond 3 Å and does not occur in a way this moiety approaches a proposed vacant site at Zn perpendicular to the plane of the  $\beta$ -diketiminate ligand.

Kinetic measurements were undertaken to better understand the hydrometallation step. Eyring analysis was conducted over a temperature range 70–100 °C. Kinetic data for the addition of **1** to **3c** was modelled as first order in **1**. The activation parameters for hydromagnesiation were found to be:  $\Delta H^\ddagger = 15.0 \pm 2.0$  kcal mol<sup>–1</sup>,  $\Delta S^\ddagger = -34.4 \pm 14.7$  cal K<sup>–1</sup> mol<sup>–1</sup> and an associated  $\Delta G_{(298\text{ K})}^\ddagger = 25.2 \pm 2.0$  kcal mol<sup>–1</sup>. Activation parameters for the closely related step of alkene insertion at transition metal centres have been derived from NMR studies. For comparison, intramolecular alkene insertion of [(Cp\*)<sub>2</sub>Nb(H)( $\eta^2$ -CH<sub>2</sub>=CH<sub>2</sub>)] has been determined to occur with  $\Delta H^\ddagger = 14.7 \pm 1.0$  kcal mol<sup>–1</sup> and  $\Delta S^\ddagger = -11.2 \pm 2.9$  cal K<sup>–1</sup> mol<sup>–1</sup>.<sup>28</sup> A related reaction of *cis*-[Rh(P<sup>i</sup>Pr<sub>3</sub>)<sub>2</sub>(H)( $\eta^2$ -CH<sub>2</sub>=CH<sub>2</sub>)] proceeds with  $\Delta H^\ddagger = 13.0$  kcal mol<sup>–1</sup> and  $\Delta S^\ddagger = -2.0$  cal K<sup>–1</sup> mol<sup>–1</sup>.<sup>29</sup> Although both processes occur with similar activation enthalpies, the entropy of activation of hydromagnesiation is large and negative, suggestive of a substantial increase in order at the transition state required for intermolecular hydromagnesiation compared to intramolecular alkene insertion at transition metals.

### C–C bond activation

Addition of **1** to methyldiene cyclobutene (**3b**) and heating (60–100 °C) gave a mixture of the ring-opened pent-5-en-1-

ylmagnesium compound **6b** and double metalation product **8b** (*vide infra*). The reaction is proposed to proceed *via* an initial hydrometallation, forming the intermediate **4b**. **4b** was not observed spectroscopically during the reaction, though DFT calculations support its formation and facile ring-opening through  $\beta$ -alkyl elimination (*vide infra*). Reaction of **1** and **3b** at 40–60 °C similarly did not show clear spectroscopic evidence of intermediate **4b**. The product of ring-opening **6b** was characterised by a diagnostic Mg–CH<sub>2</sub> unit in the <sup>1</sup>H NMR spectrum in d<sub>6</sub>-benzene solution,  $\delta_{\text{H}} = -0.25$  ppm (t, <sup>3</sup>*J*<sub>H–H</sub> = 8.1 Hz). Heteronuclear Single Quantum Coherence (HSQC) experiments were used to assign the alkene resonances at  $\delta_{\text{H}} = 4.74$ –4.87 and 5.76 ppm, and  $\delta_{\text{C}} = 113.3$  and 141.8 ppm. The infrared spectra for **6b** shows a characteristic  $\nu(\text{C}=\text{C})$  stretching frequency at 1648 cm<sup>–1</sup>. A labelling study using a Mg–D isotopomer of **1** confirmed that the deuteride is exclusively observed at the internal alkene CH position in **6b** (see ESI†). We have previously reported ring-opening of methyldiene cyclopropane (**3a**) with **1** to form **6a**.<sup>18</sup> Hence, with these Mg-reagents C–C bond activation of 3- and 4-membered hydrocarbon rings is possible, but not larger 5 or 6-membered cycloalkanes.

Addition of **2** to **3a** also leads to C–C bond activation and formation of the ring-opened product **7a**. In this case, there is spectroscopic support for the formation of the hydrometallated intermediate **5a** by a series of diagnostic resonances in the high-field region of the <sup>1</sup>H NMR spectrum. Multiplets at –0.39 to –0.36 ppm (2H) and 0.15–0.20 ppm (2H) can be assigned as the diastereotopic ring CH<sub>2</sub> groups (both resonances are bound to the same carbon environment by HSQC), while a multiplet at 0.35–0.43 ppm (1H) is assigned as the bridgehead CH group. The CH<sub>2</sub> group adjacent to the Zn centre is observed as a doublet centred at 0.24 ppm (*J* = 7.2 Hz). Selective excitation TOCSY experiments confirmed all the resonances were part of the same coupled spin system. The final reaction product **7a** was unambiguously characterised by multinuclear NMR and single crystal X-ray diffraction (Fig. 2), along with infrared spectroscopy which shows a characteristic  $\nu(\text{C}=\text{C})$  stretching frequency at 1633 cm<sup>–1</sup>. Even at elevated temperature C–C bond activation of 4-, 5- and 6-membered hydrocarbons was not

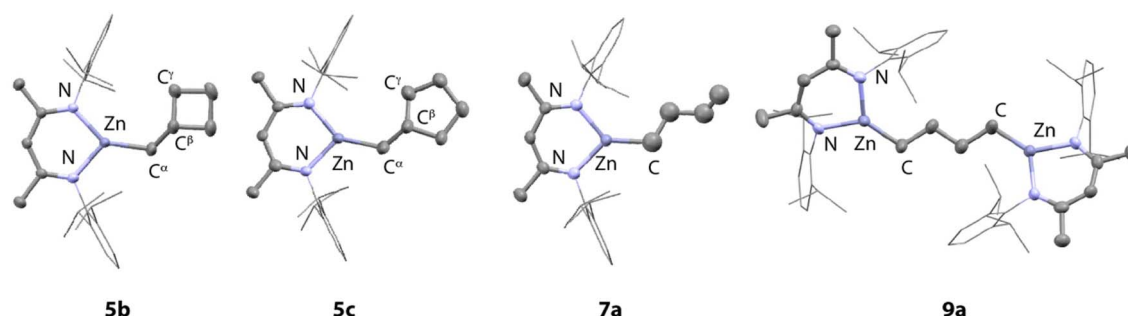


Fig. 2 Structures of **5b**, **5c**, **7a** and **9a** from single crystal X-ray diffraction experiments. Selected bond lengths (Å) and angles (°): **5b**: Zn1–N1 1.9797(13), Zn1–N2 1.9554(12), Zn1–C30 1.9697(18), C30–C31 1.504(3), N1–Zn1–N2 95.86(5), N1–Zn1–C30 124.04(8), C30–Zn1–N2 140.06(8); **5c**: Zn1–N1 1.9745(3), Zn1–N2 1.975(3), Zn1–C30 1.965(4), C30–C31 1.475(7), N1–Zn1–N2 95.52(11), N1–Zn1–C30 141.81(15), C30–Zn1–N2 122.56(15); **7a**: Zn1–N1 1.956(2), Zn1–N2 1.964(2), Zn1–C30 1.960(3), C32A–C33A 1.157(9), N1–Zn1–N2 95.83(9), N1–Zn1–C30 131.84(10), C30–Zn1–N2 132.26(10); **9a**: Zn1–N1 1.9651(16), Zn1–N2 1.9595(17), Zn1–C59 1.945(2), Zn2–N3 1.9589(17), Zn2–N4 1.9709(19), Zn2–C62 1.943(3), N1–Zn1–N2 95.47(8), N1–Zn1–C59 130.33(9), C59–Zn1–N2 134.21(8), N3–Zn2–N4 95.37(17), N3–Zn2–C62 134.54(9), C62–Zn2–N4 130.07(9).

observed with Zn. From these experiments, we can suggest that the scope of reactivity is broader for Mg compared to Zn and, given that the monomeric units of **1** and **2** are isostructural, that C–C bond activation is more facile with the more electropositive metal magnesium.

### Double metallation

In the presence of a second equivalent of the main group hydride, the products of  $\beta$ -alkyl migration are not stable. Addition of **1** to the ring-opened pent-5-en-1-ylmagnesium complex **6b** resulted in a second anti-Markovnikov hydromagnesiation reaction, yielding the 1,5-dimagnesio pentane **8b**.<sup>18,30</sup> Similarly a second hydrozincation of **7a** yields the 1,4-dizincio butane complex **9a** (Fig. 2).

### Catalytic hydrosilylation

A catalytic reaction of **3b**, two equiv. of phenylsilane, and 10 mol% **1**, led to the formation of a mixture of the hydrosilylated products **10a** and **10b** in near quantitative yield (Fig. 3). The reaction did not proceed in the absence of **1**. Following the reaction as a function of time strongly suggests that **10a** is a kinetic product that undergoes a second intramolecular hydrosilylation to give the 1-phenyl-1-silacyclohexane **10b**. **10b** could be isolated following column chromatography in 83% yield. **6b** was observed spectroscopically during the reaction procedure, supporting a mechanism involving the hydromagnesiation and  $\beta$ -alkyl migration steps identified for addition of **1** to **3b** in the absence of silane. Catalytic hydrosilylation of **3a** with **2** yielded only stoichiometric formation of the acyclic hydrosilylation product  $\text{Ph}_2\text{Si}(\text{H})(\text{CH}_2\text{CH}_2\text{CH}=\text{CH}_2)$ , suggesting that catalytic turnover is more challenging for Zn compared with Mg.

### DFT calculations

DFT calculations using the  $\omega\text{B97X-D}^{31}$  functional were used to gain further insight into the hydrometallation and  $\beta$ -alkyl migration step. A model was developed to explain the effect of both the cycloalkane ring-size and nature of the metal on reactivity. Methods were benchmarked against the solid state structures and the activation parameters from kinetics data (*vide supra*).<sup>32,33</sup> Metal atoms (Mg, Zn) were described with Stuttgart SDDAll RECPs and associated basis sets, while a hybrid basis set was used for the other atoms: 6-31g\*\* (C, H)/

6-311+g\*(N).<sup>34–36</sup> Complete potential energy surfaces for reactions of **1** and **2** with **3a–d**, along with functional testing and computational details, can be found in the ESI.†

Hydrometallation of methyldiene cycloalkanes with either **1** or **2** both proceed *via* a four membered transition state **TS-1** (Fig. 4, Table 1). No clear trend between ring size and activation barrier was noted. The nature of the main-group metal was determined to be the most important factor in determining the activation barrier for hydrometallation. Gibbs activation energies for the hydrometallation transition state **TS-1** ranged from 21.7–24.0 kcal mol<sup>−1</sup> for Mg, and 30.7–32.5 kcal mol<sup>−1</sup> for Zn (Table 1). These calculations are consistent with higher temperatures and longer reaction times observed experimentally upon reaction of **2** with methyldiene cycloalkanes compared to **1**. In all cases, the hydrometallation step is exergonic with the most energetically stable products being those in which there is relief of strain due to sp<sup>2</sup> to sp<sup>3</sup> rehybridisation on hydrometallation. For example, the difference in strain energy between methyldiene cyclopropene and cyclopropane can be estimated as 13.4 kcal mol<sup>−1</sup>.<sup>37</sup>

Natural Bond Orbital (NBO) analysis of the calculated stationary points for the hydrometallation step were undertaken (Tables S6 and S7†). Analysis of the Wiberg Bond Index (WBI) on stationary points across the pathway shows the expected decrease in C=C bond strength that occurs with loss of the unsaturated bond in **3a–b** upon addition of **1** or **2**. Take addition of **1** to **3b** as a representative example; the WBI of the breaking C=C bond decreases from **3b** → **TS-1** → **5b** (1.94 → 1.50 → 1.03). A concomitant increase in calculated bond length is observed as expected (1.32 → 1.39 → 1.52 Å).

In all cases, C–C  $\sigma$ -bond activation was calculated to proceed *via* a concerted intramolecular transition state **TS-2** best described as a  $\beta$ -alkyl migration step (Fig. 4, Table 1). For example, C–C activation of the cyclopropane ring in **3a** with **1** is calculated to occur from intermediate **4a** with a modest energy barrier ( $\Delta G^\ddagger = 19.0$  kcal mol<sup>−1</sup>) *via* **TS-2**, forming the isolable complex **6a**. Comparison of this energy barrier with that calculated for hydromagnesiation *via* **TS-1** ( $\Delta G^\ddagger = 21.7$  kcal mol<sup>−1</sup>) is consistent with the lack of spectroscopic observation of the intermediate **4a** during the reaction course.

The computational model can be used to explain the effects of both ring-size and influence of metal on the  $\beta$ -alkyl migration step. The activation barriers for  $\beta$ -alkyl migration increase with increasing ring size of cycloalkane ring *i.e.* 3 < 4 < 5 < 6. In all

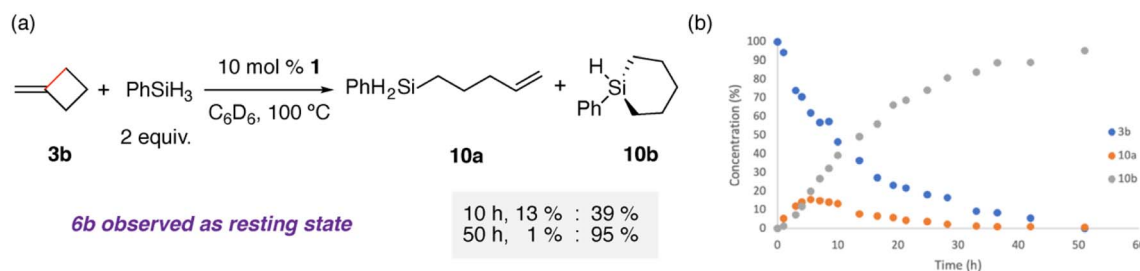


Fig. 3 (a) Catalytic hydrosilylation of **3b** with **1**, NMR yields for key time points noted; (b) reaction progress plot for catalytic hydrosilylation of **3b** with **1** at 100 °C.



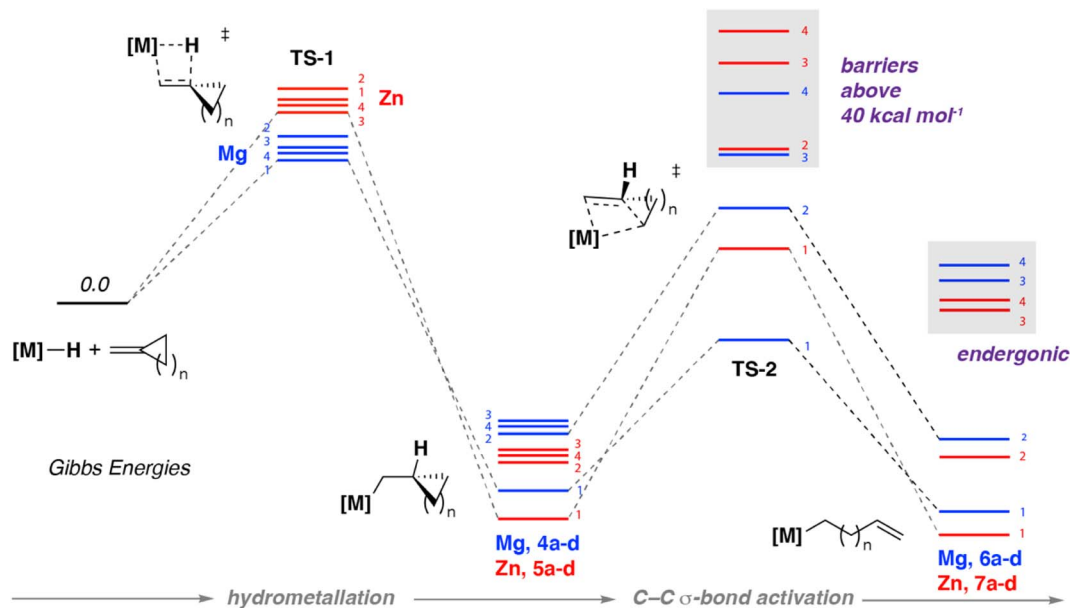


Fig. 4 Calculated reaction pathway for hydrometallation and  $\beta$ -alkyl migration ( $\omega$ B97XD). Each stationary point is marked with the value of  $n$  ( $n = 1, 2, 3, 4$ ) for hydrocarbon ring size and coded for Mg (blue) and Zn (red).

**Table 1** Calculated local barriers for hydrometallation of methylenecycloalkanes and  $\beta$ -alkyl migration at Mg and Zn. Gibbs energies values in kcal mol $^{-1}$

M =		Hydrometallation		$\beta$ -Alkyl migration	
Mg					
$N$		TS-1	4a-d	TS-2	6a-d
1		21.7	-24.7	19.0	-3.1
2		24.0	-15.6	28.0	-0.5
3		22.4	-14.8	40.7	19.0
4		22.2	-15.5	53.6	23.4

M =		Hydrometallation		$\beta$ -Alkyl migration	
Zn					
$N$		TS-1	5a-d	TS-2	7a-d
1		32.2	-27.6	35.2	-2.8
2		32.5	-18.2	44.4	0.8
3		30.7	-16.8	56.7	19.4
4		30.9	-17.5	70.1	23.0

cases these barriers are higher for Zn than they are for Mg. Hence, while  $\beta$ -alkyl migration for 3-membered ring systems is just about accessible for both metals (Mg,  $\Delta G^\ddagger = 19$  kcal mol $^{-1}$ ; Zn,  $\Delta G^\ddagger = 35.2$  kcal mol $^{-1}$ ), for 4-membered rings only the Mg analogue is predicted to facilitate  $\beta$ -alkyl migration under the experimental conditions (Mg,  $\Delta G^\ddagger = 28.0$  kcal mol $^{-1}$ ; Zn,  $\Delta G^\ddagger = 44.4$  kcal mol $^{-1}$ ). For both metals,  $\beta$ -alkyl migration of substrates containing five- and six-membered systems by TS-2 have energy barriers that are inaccessible under the reaction conditions ( $\Delta G^\ddagger > 40$  kcal mol $^{-1}$ ). Furthermore, the overall ring

opening process for larger ring sizes are calculated to be endergonic, so would be expected to be reversible even if the activation barriers were traversed. The ring strain energies of methylenecyclopropane, cyclobutene, cyclopentane and cyclohexane have been determined as 40.9, 26.9, 6.1, and -1.1 kcal mol $^{-1}$  respectively.<sup>38</sup> Our calculations are consistent with relief of ring-strain as a definitive factor in driving the thermodynamics of C-C bond activation.

The C-C  $\sigma$ -bond activation step can be understood in more detail through further consideration and analysis of transition state. In all cases, breaking of the M-C $_{\alpha}$ , and making of the M-C $_{\gamma}$  bond accompanies C $_{\beta}$ -C $_{\gamma}$  bond activation. As a result, the C $_{\alpha}$ =C $_{\beta}$ ...C $_{\gamma}$  motif adopts an electronic structure reminiscent of an allyl ligand in the TS (Fig. 5a). For example, TS-2 when M = Mg and  $n = 1$  has a short C $_{\alpha}$ =C $_{\beta}$  bond length of 1.42 Å, stretched C $_{\beta}$ -C $_{\gamma}$  bond of 1.94 Å, and even, near symmetric, Mg-C $_{\alpha}$  and Mg-C $_{\gamma}$  distances of 2.22 and 2.26 Å respectively. Charge localisation occurs across the allyl-like moiety, but primarily at the terminal carbons, C $_{\alpha}$  (-1.01) and C $_{\gamma}$  (-0.94), rather than C $_{\beta}$  (-0.18). AIM calculations capture bond paths between both C $_{\alpha}$  and C $_{\gamma}$  with Mg, but not between C $_{\beta}$  and C $_{\gamma}$  in the breaking bond. Wiberg bond indices from NBO provide a similar picture of electron distribution in this TS, with partial double bond character in the C $_{\alpha}$ =C $_{\beta}$  unit (1.42) and a weakened C $_{\beta}$ ...C $_{\gamma}$  bond (0.57). Second order perturbation from the NBO calculations show donation of electron density from the C $_{\alpha}$  atom (35.2 kcal mol $^{-1}$ ), C $_{\beta}$ -C $_{\gamma}$  bond (17.5 kcal mol $^{-1}$ ), C $_{\alpha}$ -C $_{\beta}$  bond (2.6 kcal mol $^{-1}$ ) and C $_{\gamma}$  atom (1.4 kcal mol $^{-1}$ ) to Mg. An NCI plot further supports the proposed allyl character of the hydrocarbon ligand, as it shows attractive interactions between each carbon atom and the magnesium site (Fig. 5b).

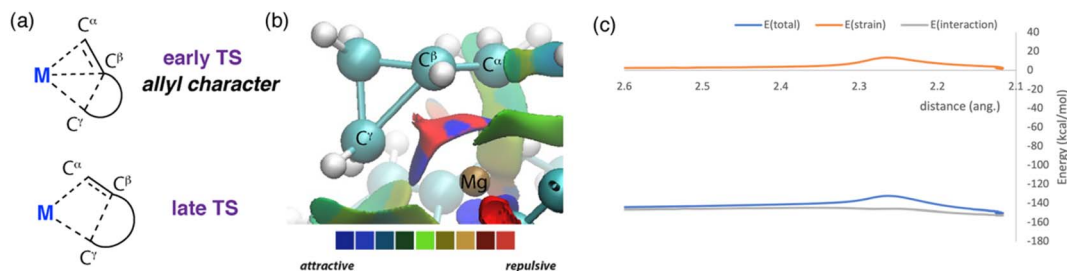


Fig. 5 (a) Depiction of allyl like ligand binding to the metal centre. (b) NCI plot for TS-2 (M = Mg,  $n = 1$ ). (c) activation strain analysis (ASA): TS-2 (M = Mg,  $n = 1$ ) along the Mg-C<sub>γ</sub> bond. ASA plots for complete TS-2 series can be found in the ESI (Table S8, Fig. S19–S36†).

## Activation strain analysis

While relief of ring strain is clearly an important thermodynamic driving force for these reactions, it is not immediately clear if this is also a factor in determining the kinetics of C–C bond activation. Activation Strain Analysis (ASA) was performed to address this question.<sup>39–41</sup> This approach interrogates energy changes on the potential energy surface around the transition state, at the simplest level deconvoluting the total energy of the system into the interaction energy  $\Delta E_{\text{int}}(\zeta)$  between two fragments and the strain energy  $\Delta E_{\text{strain}}(\zeta)$  required to distort said fragments along the potential energy surface. Typically, ASA is applied to bimolecular reactions, although there are examples of unimolecular systems where this approach has provided useful insight.<sup>42,43</sup> In intramolecular cases, the choice of fragments has been proposed to be crucial in obtaining meaningful information on the factors that impact reactivity. Here the interaction of the cycloalkane fragment (e.g. C<sub>4</sub>H<sub>7</sub> or C<sub>5</sub>H<sub>9</sub>) with the metal fragment [M{(NArCMe)<sub>2</sub>CH<sub>3</sub>}] was considered (M = Mg, Zn; Ar = 2,6-di-iso-propylphenyl). Hence, our ASA calculations should provide insight into the strain required to distort each of these fragments to the TS geometry, and the difference in interaction energies (i.e. the binding energy) between the metal and the hydrocarbon ligand as the TS is approached.

Activation strain analysis on the potential energy surface associated with  $\beta$ -alkyl migration transition state TS-2 suggests that there is only a slight difference in the contribution from strain energy in these two reactions (Fig. 5c). For both systems, the reaction strain energy  $\Delta E_{\text{strain}}(\zeta)$  reaches a maximum at the transition state. For Mg, there is little difference in the strain energy,  $\Delta\Delta E_{\text{strain}}^\ddagger$  from reactant to transition state, TS-2 ( $n = 1$ , 12.0 kcal mol<sup>−1</sup>;  $n = 2$ , 11.9 kcal mol<sup>−1</sup>). Nearly all the contribution to the strain energy is from distortion of the hydrocarbon fragment. On further inspection of the transition state geometries this conclusion becomes more intuitive, there are only small distortions in bond angles in the ring systems of these structures when compared to the parent cycloalkanes. Hence, relief of ring strain does not occur at the transition state but rather later along the reaction coordinate as the system progresses toward the products. The interaction energy  $\Delta E_{\text{int}}(\zeta)$  is negative and relatively flat across the reaction coordinate. This is perhaps expected, as the calculated data points describe a concerted bond breaking and bond making event in which stabilising interactions from forming bonds are counterbalanced by destabilising

interactions from breaking bonds. From reactant to transition state, the change in interaction energy is positive, suggestive of a less stabilising interaction between the metal site and hydrocarbon fragment as the TS is approached. For the Mg system, comparing  $\Delta\Delta E_{\text{int}}^\ddagger$  for TS-2 ( $n = 1$ , 1.1 kcal mol<sup>−1</sup>;  $n = 2$ , 7.7 kcal mol<sup>−1</sup>) suggests that the origin of the higher activation energy for 4-membered vs. 3-membered rings can be traced to a weaker binding of the hydrocarbon to the metal. Based on these calculations, it can be speculated that more facile activation of the smaller ring sizes is not a consequence of relief of ring strain in the transition state, but rather a more stabilising interaction of the allyl type ligand with the metal at the TS.

Polarisation and charge delocalisation across the C<sub>α</sub>=C<sub>β</sub>...C<sub>γ</sub> moiety may also play a role in the differences in reactivity for Mg and Zn. Transition states for C–C bond activation are calculated to be higher in energy for Zn than for Mg across the whole series. For Zn, activation strain analysis again suggests that there is little difference in the relief of ring strain on going from reactant to the transition state  $\Delta\Delta E_{\text{strain}}^\ddagger$  for TS-2 ( $n = 1$ , 11.1 kcal mol<sup>−1</sup>;  $n = 2$ , 12.9 kcal mol<sup>−1</sup>). Rather the interaction energy is again the key factor at play.  $\Delta\Delta E_{\text{int}}^\ddagger$  for TS-2 ( $n = 1$ , 8.1 kcal mol<sup>−1</sup>;  $n = 2$ , 19.7 kcal mol<sup>−1</sup>) is less destabilising for the smaller ring size. In addition,  $\Delta\Delta E_{\text{int}}^\ddagger$  values for TS-2 for both ring sizes are less destabilising for Mg compared to Zn. The Mg site is both larger and more electropositive than Zn ( $r_{\text{cov}}$  Mg = 1.39, Zn = 1.18 Å;  $\chi_{\text{p}}$  Mg = 1.31, Zn = 1.65). As such it is likely better placed to polarise the C<sub>α</sub>=C<sub>β</sub>...C<sub>γ</sub> moiety and stabilise the resultant fragment through electrostatic interactions with all three carbon centres. The Zn atom is less well suited to accommodate coordination of all three carbon atoms involved in C–C bond activation. This supposition is supported by the calculated TS geometries for Zn which show a greater asymmetry in the Zn–C<sub>α</sub> and Zn–C<sub>γ</sub> distances compared to Mg analogues. For example, in TS-2 ( $n = 1$ ) there is a  $\Delta = 0.22$  Å difference in these values for Zn, whereas it is only  $\Delta = 0.05$  Å for Mg. We speculate these differences make an important contribution to raising the energy of the C–C bond activation step for Zn relative to Mg.

## Conclusions

In summary, C–C  $\sigma$ -bond activation of strained cyclic hydrocarbons has been observed to occur at both Mg and Zn metal centres. While ring-opening of both 3- and 4-membered rings



was observed with Mg reagents, isostructural Zn species were only capable of reacting with smaller 3-membered rings. DFT calculations, benchmarked against the experiment data and activation parameters from kinetics, support a mechanism for C–C  $\sigma$ -bond activation involving  $\beta$ -alkyl migration. While relief of ring strain provides a thermodynamic driving force for  $\beta$ -alkyl migration, activation strain analysis suggests that it does not lower the barrier for breaking the C–C  $\sigma$ -bond by an appreciable amount. Rather, the interaction energy between the metal and the hydrocarbon fragment at the transition state is likely the key contributor to determining the kinetic barrier to  $\beta$ -alkyl migration. This is more favourable for smaller ring sizes (3 vs. 4) and for the more electropositive metal (Mg vs. Zn). In combination, the analysis suggests the  $\beta$ -alkyl migration at main group centres should become more favourable for systems in which the metal can polarise the hydrocarbon fragment, and the hydrocarbon fragment can best accommodate and delocalise the associated charge.

## Data availability

Experimental procedures, details of the calculations, and additional data can be found in the ESI (pdf).† X-ray data is available in .cif format.

## Author contributions

JP, AP, and AV conducted experimental work. JP conducted all computational work. AP solved and refined all single crystal XRD data. JP, AP, and MRC wrote the manuscript. All authors agreed on the final version of the manuscript.

## Conflicts of interest

There are no conflicts to declare.

## Acknowledgements

We thank Imperial College London for the award of a Schrödinger's Scholarship (JP). We thank Pete Haycock for NMR experiments. Horizon 2020 is acknowledged for funding of a MSCA fellowship (AP).

## References

- 1 B. Wang, M. A. Perea and R. Sarpong, *Angew. Chem., Int. Ed.*, 2020, **59**, 18898–18919.
- 2 M. Murakami and N. Ishida, *J. Am. Chem. Soc.*, 2016, **138**, 13759–13769.
- 3 S. J. Blanksby and G. B. Ellison, *Acc. Chem. Res.*, 2003, **36**, 255–263.
- 4 V. M. Benitez, J. M. Grau, J. C. Yori, C. L. Pieck and C. R. Vera, *Energy Fuels*, 2006, **20**, 1791–1798.
- 5 F. P. Guengerich and F. K. Yoshimoto, *Chem. Rev.*, 2018, **118**, 6573–6655.
- 6 M. Gozin, A. Welsman, Y. Ben-David and D. Milstein, *Nature*, 1993, **364**, 699–701.
- 7 C. Jun, *Chem. Soc. Rev.*, 2004, **33**, 610–618.
- 8 Y. Xia, G. Lu, P. Liu and G. Dong, *Nature*, 2016, **539**, 546–550.
- 9 L. Souillart and N. Cramer, *Chem. Rev.*, 2015, **115**, 9410–9464.
- 10 M. E. O'Reilly, S. Dutta and A. S. Veige, *Chem. Rev.*, 2016, **116**, 8105–8145.
- 11 K. Ziegler, *Angew. Chem.*, 1956, **68**, 721–729.
- 12 D. Dakternieks, A. E. K. Lim and K. F. Lim, *Chem. Commun.*, 1999, **15**, 1425–1426.
- 13 R. Y. Kong and M. R. Crimmin, *Angew. Chem., Int. Ed.*, 2021, **60**, 2619–2623.
- 14 X. Zhang and L. L. Liu, *Angew. Chem., Int. Ed.*, 2022, **134**, 2–7.
- 15 K. Koshino and R. Kinjo, *J. Am. Chem. Soc.*, 2020, **142**, 9057–9062.
- 16 J. Hicks, P. Vasko, J. M. Goicoechea and S. Aldridge, *J. Am. Chem. Soc.*, 2019, **141**, 11000–11003.
- 17 J. G. M. Morton, M. A. Dureen and D. W. Stephan, *Chem. Commun.*, 2010, **46**, 8947–8949.
- 18 R. Y. Kong and M. R. Crimmin, *J. Am. Chem. Soc.*, 2020, **142**, 11967–11971.
- 19 S. P. Green, C. Jones and A. Stasch, *Angew. Chem., Int. Ed.*, 2008, **47**, 9079–9083.
- 20 L. Garcia, C. Dinoi, M. F. Mahon, L. Maron and M. S. Hill, *Chem. Sci.*, 2019, **10**, 8108–8118.
- 21 J. Spielmann, D. Piesik, B. Wittkamp, G. Jansen and S. Harder, *Chem. Commun.*, 2009, **23**, 3455–3456.
- 22 G. J. Baker, A. J. P. White, I. J. Casely, D. Grainger and M. R. Crimmin, *ChemRxiv*, 2022, preprint, DOI: [10.26434/chemrxiv-2022-3tcn2-v2](https://doi.org/10.26434/chemrxiv-2022-3tcn2-v2).
- 23 M. Cheng, D. R. Moore, J. J. Reczek, B. M. Chamberlain, E. B. Lobkovsky and G. W. Coates, *J. Am. Chem. Soc.*, 2001, **123**, 8738–8749.
- 24 S. P. Sarish, D. Schaffner, Y. Sun and W. R. Thiel, *Chem. Commun.*, 2013, **49**, 9672–9674.
- 25 J. Prust, A. Stasch, W. Zheng, H. W. Roesky, E. Alexopoulos, I. Usón, D. Böhler and T. Schuchardt, *Organometallics*, 2001, **20**, 3825–3828.
- 26 T. Pietrzak, I. Justyniak, M. Kubisiak, E. Bojarski and J. Lewiński, *Angew. Chem., Int. Ed.*, 2019, **58**, 8526–8530.
- 27 S. C. Cole, M. P. Coles and P. B. Hitchcock, *Organometallics*, 2004, **23**, 5159–5168.
- 28 N. M. Doherty and J. E. Bercaw, *J. Am. Chem. Soc.*, 1985, **107**, 2670–2682.
- 29 H. C. Foley, S. J. Decanio, K. D. Tau, K. J. Chao, J. H. Onuferko, C. Dybowski and B. C. Gates, *J. Am. Chem. Soc.*, 1983, **105**, 3074–3082.
- 30 K. Yuvaraj, I. Douair, L. Maron and C. Jones, *Chem.–Eur. J.*, 2020, **26**, 14665–14670.
- 31 J. Da Chai and M. Head-Gordon, *J. Chem. Phys.*, 2008, **128**, 084106.
- 32 M. Garçon, N. W. Mun, A. J. P. White and M. R. Crimmin, *Angew. Chem., Int. Ed.*, 2021, **60**, 6145–6153.
- 33 M. J. Butler, A. J. P. White and M. R. Crimmin, *Angew. Chem., Int. Ed.*, 2016, **55**, 6951–6953.
- 34 W. J. Hehre, R. Ditchfield and J. A. Pople, *J. Chem. Phys.*, 1972, **56**, 2257–2261.
- 35 P. C. Hariharan and J. A. Pople, *Theor. Chim. Acta*, 1973, **28**, 213–222.



- 36 T. Clark, J. Chandrasekhar, G. W. Spitznagel and P. v R. Schleyer, *J. Comput. Chem.*, 1983, **4**, 294–301.
- 37 K. B. Wiberg, *Angew. Chem., Int. Ed.*, 1986, **25**, 312–322.
- 38 T. Dudev and C. Lim, *J. Am. Chem. Soc.*, 1998, **120**, 4450–4458.
- 39 D. Svatunek and K. N. Houk, *J. Comput. Chem.*, 2019, **40**, 2509–2515.
- 40 P. Vermeeren, S. C. C. van der Lubbe, C. Fonseca Guerra, F. M. Bickelhaupt and T. A. Hamlin, *Nat. Protoc.*, 2020, **15**, 649–667.
- 41 F. M. Bickelhaupt and K. N. Houk, *Angew. Chem., Int. Ed.*, 2017, **56**, 10070–10086.
- 42 I. Fernández, F. M. Bickelhaupt and F. P. Cossío, *Chem.–Eur. J.*, 2014, **20**, 10791–10801.
- 43 I. Fernández, F. M. Bickelhaupt and F. P. Cossío, *Chem.–Eur. J.*, 2012, **18**, 12395–12403.

